AIP | Journal of Applied Physics

# Diversity of electronic transitions and photoluminescence properties of p-type cuprous oxide films: A temperature-dependent spectral transmittance study

W. L. Yu, Y. Z. Lin, X. W. Zhu, Z. G. Hu, M. J. Han, S. S. Cai, L. L. Chen, and H. H. Shao

Citation: Journal of Applied Physics **117**, 045701 (2015); doi: 10.1063/1.4906405
View online: http://dx.doi.org/10.1063/1.4906405
View Table of Contents: http://scitation.aip.org/content/aip/journal/jap/117/4?ver=pdfcov
Published by the AIP Publishing



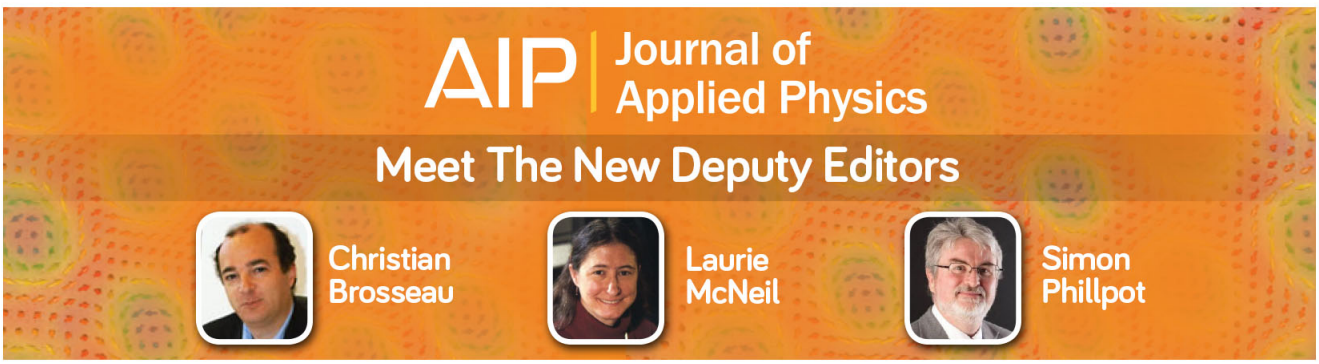

# Diversity of electronic transitions and photoluminescence properties of *p*-type cuprous oxide films: A temperature-dependent spectral transmittance study

W. L. Yu (余温雷),[1,a)] Y. Z. Lin (林晔智),[1] X. W. Zhu (朱秀委),[1] Z. G. Hu (胡志高),[2,a)]
M. J. Han (韩美杰),[3] S. S. Cai (蔡双双),[1] L. L. Chen (陈亮亮),[1] and H. H. Shao (邵和鸿)[1]
[1]*Department of Biomedical Engineering, Wenzhou Medical University, Zhejiang 325035, People's Republic of China*
[2]*Key Laboratory of Polar Materials and Devices, Ministry of Education, Department of Electronic Engineering, East China Normal University, Shanghai 200241, People's Republic of China*
[3]*School of Electrical Engineering, Shanghai Dianji University, Shanghai 201306, People's Republic of China*

(Received 16 November 2014; accepted 10 January 2015; published online 22 January 2015)

Cuprous oxide films have been deposited on quartz substrates by a sol-gel method under various annealing temperatures. The X-ray diffraction analysis and Raman scattering show that all the films are of pure $Cu_2O$ phase. From comparison of photoluminescence with 488 and 325 nm laser excitations, the electronic transition energies and intensities present the annealing-temperature dependent behavior. The electronic band structures of the $Cu_2O$ film annealed at 800 °C, especially for the contribution of exciton series and high energy transitions, have been investigated by temperature dependent transmittance. The extracted refraction index and the high frequency dielectric constant both abruptly decrease until the temperature rises up to 100 K. Six transitions can be clearly identified and the red shift trend of $E_{o3}$-$E_{o5}$ transition energies with increasing the temperature can be found. Moreover, the anomalous behavior takes place at about 200 K from the $E_{o6}$ transition. The singularities indicate that the change in the crystalline and electronic band structure occurs as the temperature near 100 K and 200 K for the film. © *2015 AIP Publishing LLC*.
[http://dx.doi.org/10.1063/1.4906405]

## I. INTRODUCTION

Cuprous oxide ($Cu_2O$) is a promising multifunctional material in catalysts, gas sensors, electronics, lithium ion batteries, and solar energy conversion; it can be used as an environmentally friendly *p*-type semiconductor material with a direct band gap of 1.9–2.2 eV.[1–4] As a prospective candidate in visible photocatalysis applications, its photocatalytic performance is limited by the recombination of the photoexcited electrons and holes.[5] The attractiveness of $Cu_2O$ as a photovoltaic material lies in the fact that the constituent materials are nontoxic and abundantly available. Moreover, the $Cu_2O$ has a high optical absorption coefficient in the visible regions and low cost production.[6] There are numerous reports on the exploitation of $Cu_2O$ as an active layer for solar cells.[7,8] Even though it has a theoretical conversion efficiency of around 20%, actual efficiencies reported so far are around 2%.[7] This is often due to low open-circuit voltages resulting from rapid interfacial recombination.[9] As one of the most key candidates for solar cell material, optical properties and crystalline quality affect both the heat losses and gains.[10] Therefore, it is necessary to prepare pure $Cu_2O$ nanocrystals to further examine the crystal structure and characterize the electronic properties. It can be found that Raman spectra from $Cu_2O$ material provide some anomalies for the thermal behavior at 90 and 180 K, which might be related to structural and/or electronic changes.[11] Additionally, negative thermal expansion (NTE) behavior of cubic $Cu_2O$ has been calculated, which is in fair agreement with the available experimental data up to 200 K.[12] The origin of the discrepancies between theoretical and experimental results for NTE as well as Hall mobilities at temperatures above 200 K is currently unresolved.[12,13] These phenomena make us pay attention to the variation on physical picture from $Cu_2O$ as a function of temperature.

Considering the potential applications of copper-based materials, many kinds of morphologies have been reported, such as wires, monodisperse nanocubes, octahedral nanocages, hollow nanospheres, and so forth.[14–16] The effect of band gap variation and surface reconstruction on the optoelectronic properties of $Cu_2O$ nanoparticles are understood by altering the size of nanoparticles with different shape symmetries.[16] The electronic and optical response behaviors of $Cu_2O$ films are not only dependent on preparation methods and various morphologies, but also sensitive to external perturbations, such as temperature, pressure, and optical fields. Early researches indicated that the photoluminescence (PL) peaks at 2.26 and 2.71 eV correspond to the yellow and the green spectral ranges. Since the PL also has a blue luminescence, moderate control of the peak intensities in the three colors provides good motivation for potential applications in the white-light-emitting devices.[17] The number of optical transition is related to electronic band structure of the $Cu_2O$ films. Based on the theoretical calculations and experimental observations, many transitions at the photon energy from

a)Authors to whom correspondence should be addressed. Electronic addresses: wenleiyu@wmu.edu.cn and zghu@ee.ecnu.edu.cn. Tel.: +86-21-54345150. Fax: +86-21-54345119.

 

ultraviolet to near-infrared and the assignments are widely acceptable.[18–20] However, there are few systematical reports concerning the dielectric functions and electronic transition at low temperatures, especially for the higher-order interband transitions. On the basis of the previous work on the $Cu_2O$ nanostructures,[21] temperature-dependent Raman intensity ratios have been investigated and the anomalous behaviors in the vicinity of 200 K can be found. Note that the Raman spectra can provide some invaluable information on the crystal structure for $Cu_2O$ material. In addition, temperature dependence of the electronic transitions can also provide the critical information about the electron-phonon interactions and collective excitations for semiconductor $Cu_2O$ material. It is important in analysis of physical properties behind the anomalous behavior and understanding the role of the electronic contribution to the optical properties. Therefore, it is desirable to carry out a detail study regarding the essential effects of temperature on dielectric functions and high energy transitions, in order to detect possible anomalies in the $Cu_2O$ structure.

In this article, the dielectric functions, optical band gap (OBG), and electronic transitions of the $Cu_2O$ films grown quartz substrates have been investigated by Raman scattering, PL, and spectral transmittance technique. We compared with PL spectra under 325 and 488 nm laser excitations at room temperature (RT). A dielectric function theoretical model is presented to reproduce the experimental transmittance spectra well. The temperature influences on the electronic band structures, especially for anomalies at about 100 and 200 K, have been discussed in detail.

## II. EXPERIMENTAL DETAILS

### A. Fabrication of the $Cu_2O$ films

The sol-gel method is known to be effective chemical processes for the synthesis of $Cu_2O$ nanoparticles. The characteristics of the final products, such as crystallite size and distribution, can be suitably control by a proper choice of the molecular precursors and of the annealing conditions. It was focused on the chemical and microstructural evolution of the $Cu_2O$ systems as a function of the annealing treatment, e.g., temperature, time, and atmosphere.[22] The physical behaviors of the $Cu_2O$ are sensitive to the grown situation, experimental condition, and substrate temperature. Nanocrystalline $Cu_2O$ film studied in this work was prepared on quartz substrate by the sol-gel method.[23] Copper acetate hydrate $[Cu(C_2H_3O_2)_2 \cdot H_2O$, 99%, 0.4 g] was dissolved in anhydrous ethanol ($C_2H_6O$, 99.7%, 20 ml) under magnetic stirring. After the solution was stable and became transparent and homogeneous, the 0.1 M precursors were spin-coated onto quartz substrate at the speed of 4000 rpm for 20 s. The deposited film was dried at 300 °C for 300 s to remove residual organic compounds, following annealing at 800, 850, and 900 °C for 15 min in $N_2$ with a flow of 2.0 l/min by a rapid thermal annealing procedure, respectively.

### B. Sample characterizations

The crystalline structures, surface morphology, and cross section microstructure of the $Cu_2O$ films under different annealing temperatures were analyzed by X-ray diffraction (XRD) using Cu $K\alpha$ radiation (D/MAX-2550 V, Rigaku Co.) and scanning electron microscope (SEM, S-3000 N, Philips XL30FEG). In the XRD measurement, a vertical goniometer (Model RINT2000) and continuous scanning mode ($\theta$–$2\theta$) were selected with an scanning rate of 10°/min and interval of 0.02°. From Hall measurements by ver der Pauw method at RT, the carriers in the $Cu_2O$ film annealed at 800 °C are found to be positive, showing *p* type behavior with Hall mobility of 31.7 $cm^2V^{-1}s^{-1}$.[21] The PL spectra and Raman scattering were carried out at RT by a Jobin-Yvon LabRAM HR 800 UV micro-Raman instrument with a $Ar^+$ (488 nm) laser as excitation sources. While the PL spectra also were recorded with a He-Cd laser as the excited light, which is operated at the wavelength of 325 nm (3.82 eV). The spectral transmittance experiments were done with a double beam spectrophotometer (PerkinElmer Lambda 950) from 190 to 2650 nm (0.47–6.5 eV) with a spectral resolution of 2 nm. The film grown at 800 °C was mounted into an optical cryostat (Janis SHI-4-1) for low temperature measurements from 8 to 300 K.

## III. RESULTS AND DISCUSSIONS

### A. Structural analysis and lattice vibrations

There are two diffraction peaks observed from the XRD patterns for the $Cu_2O$ films at different annealing temperatures (not shown), which are indexed to the (111) and (200) peaks of cubic $Cu_2O$. No characteristic XRD peaks arising from impurities are detected, indicating that all samples are composed of pure $Cu_2O$ phase. With increasing annealing temperature, the lattice parameters of *a* are about 4.251, 4.241, and 4.237 Å from the diffraction angle of the (200) peak, respectively. The corresponding values of *d*-spacing ($d_{111}$) are calculated to 2.458, 2.451, and 2.450 Å, respectively. The reductions of above parameters may indicate the more lattice distortion in the crystal grown under the higher annealing temperature. As seen in Figure 1, the thicknesses of the films are evaluated to about 100 nm. The films have a fluctuating surface and show more fuzzy morphology with increasing annealing temperature. In order to further confirm the crystallinity, composition, and structure of the $Cu_2O$ films, Figure 2 presents a nine-peak Gaussian fit of the Raman spectra recorded in the range of 50–900 $cm^{-1}$ for the samples. It includes Raman-active ($\Gamma_{25^+}$), infrared-active symmetry ($\Gamma^{(1)}_{15^-}$, $\Gamma^{(2)}_{15^-}$), and other symmetry selection rule forbidden modes ($\Gamma_{25^-}$, $\Gamma_{2^+}$ and $\Gamma_{12^-}$). The forbidden modes become allowed through defects or an intrinsic selection-rule violation mechanism in the pure crystal.[11] Lattice dynamical calculations show that Cu-dominated modes are responsible for the low frequency part, modes above 60 meV (484 $cm^{-1}$) are oxygen dominated.[12,24] The copper site exhibits a preferential vibration in the direction perpendicular to the linear O-Cu-O bond. This could explain the NTE through the rotation of $Cu_4O$ tetrahedra, which can shorten O-O distance.[25] It can be found that the peak positions of the above phonon modes are very close to those of the typical phonon vibrations for $Cu_2O$ crystal.[11,26,27] The Raman data further support the formation of $Cu_2O$ phase, which are in agreement with the XRD

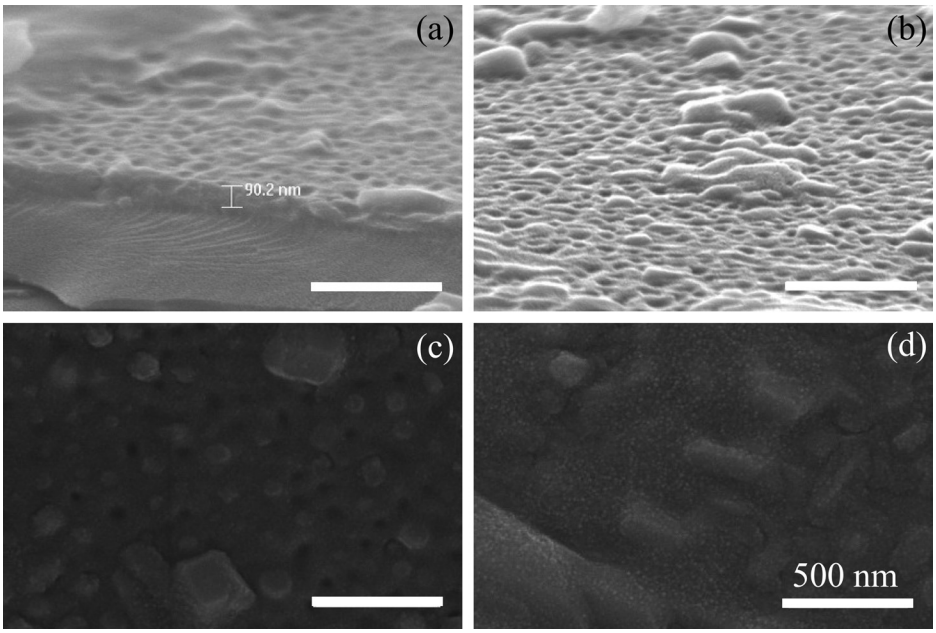


FIG. 1. The scanning electron microscopy images of the $Cu_2O$ films on quartz substrates annealed under (a) and (b) 800 °C, (c) 850 °C, and (d) 900 °C, respectively. The cross-section microstructure indicates that the thickness of the film deposited under annealing temperature of 800 °C is estimated to be about 90 nm.

experiments. The relatively minor changes in the Raman peak positions with different annealing suggest that the films are unlikely to have undergone further oxidation and the films are relatively stable morphologically with the $Cu_2O$ phase.[28]

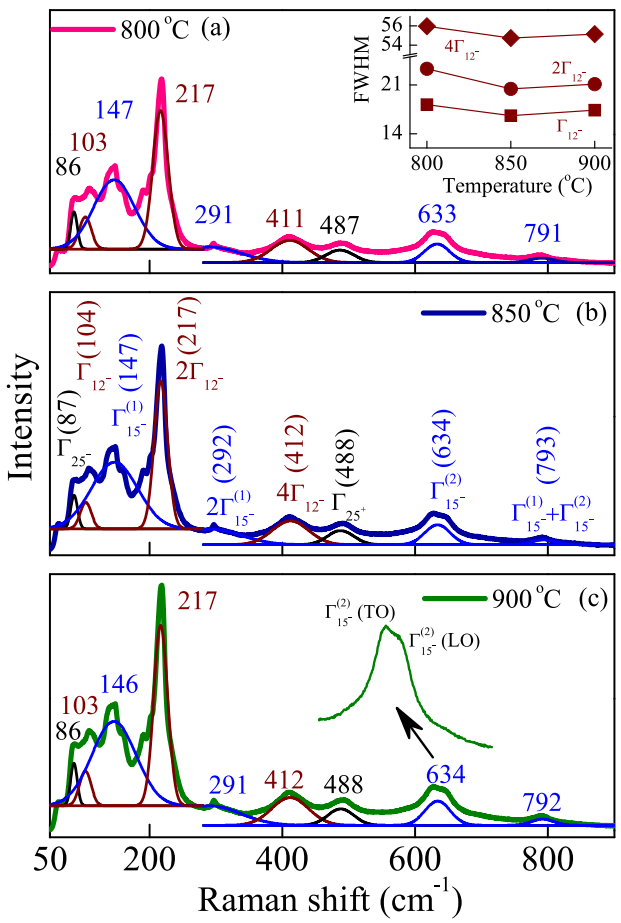


FIG. 2. Raman spectra of the $Cu_2O$ films deposited under annealing temperature of (a) 800 °C, (b) 850 °C, and (c) 900 °C, respectively. Each vibration mode has been labeled. The inset of (a) shows the FWHM of corresponding phonon modes. The enlarged frequency region of 650–750 $cm^{-1}$ from the Raman scattering is plotted in the inset of (c).

On the other hand, experimentally, it has been found that the $\Gamma_{12^-}$ phonon has the strongest coupling to the yellow exciton.[29] In our case with the 488 nm excitation, the $\Gamma_{12^-}$ (104 $cm^{-1}$), $2\Gamma_{12^-}$ (217 $cm^{-1}$), and $4\Gamma_{12^-}$ (412 $cm^{-1}$), neither infrared nor Raman mode, can be observed. The full width at half-maximum (FWHM) as functions of anneal temperature for above modes is shown in the inset of Figure 2(a). It is reasonable that the FWHM variation with the temperature of $\Gamma_{12^-}$ shares with the same behavior for ones of $2\Gamma_{12^-}$ and $4\Gamma_{12^-}$ due to the second/fourth-order response. The most intense Raman signal for all $Cu_2O$ films at RT is the second-order overtone $2\Gamma_{12^-}$, indicating the existence of strong electron-phonon coupling mediated by Fröhlich interaction in the films composed of the $Cu_2O$ phase.[30] Other weak scattering from Raman forbidden first-order modes (such as those at 104 and 634 $cm^{-1}$) could be due to intrinsic selection rule violation mechanisms in pure $Cu_2O$ crystal.[27] The low frequency vibrational mode $\Gamma_{25^-}$ (81 $cm^{-1}$) represents a rigid rotation of the $Cu_4O$ tetrahedron around oxygen atoms. It is arising from the transverse vibration of Cu atoms, which partially contributes to the NTE.[12,31] While the phonon mode at 104 $cm^{-1}$ is a twisting of the $Cu_4O$ tetrahedron around the *c* axis and it also leads to the NTE because of the tension mechanism of the O-Cu-O bonds.[31] The only Raman-active mode $\Gamma_{25^+}$ (488 $cm^{-1}$) is assigned to relative motion of the two simple cubic O lattices. It can participate in one-phonon non-resonant Raman scattering because of parity selection rules, and can appear at the same frequency for different excitations (488 nm and 514.5 nm).[11]

Moreover, the polar mode $\Gamma_{15^-}$ is of particular interest, because the LO phonon carries an electric field associated with Fröhlich interaction. It produces the LO-TO splitting and leads to additional scattering for the LO component.[32] The LO-TO splitting of 2.5 $cm^{-1}$ and 30 $cm^{-1}$ for the lower-frequency $\Gamma^{(1)}_{15^-}$ and higher-frequency $\Gamma^{(2)}_{15^-}$ modes has been reported, respectively.[32] In the present works, however, it is impossible to unambiguously separate the TO and LO components from the $\Gamma^{(1)}_{15^-}$ and $\Gamma^{(2)}_{15^-}$ modes using Gaussian

fitting. Fortunately, the extracted energy (147 $cm^{-1}$, 18.2 meV) for only LO scattering $\Gamma_{15^-}^{(1)}$ (LO) at RT is slightly less than the reported value (19.1 meV at 10 K). And the $\Gamma_{15^-}^{(2)}$ (TO, 634 $cm^{-1}$, 78.6 meV) coincides with the literature data (78.5 meV at 10 K).[33] Note that the TO and LO components of the $\Gamma_{15^-}^{(2)}$ could be distinguished from eyes in the Raman scattering (inset of Figure 2(c)). As a rough comparison, the intensity of the $\Gamma_{15^-}^{(2)}$ (TO) mode is close to or slightly larger than that of LO component for all the $Cu_2O$ films. Nevertheless, the enhancement of two LO components [$\Gamma_{15^-}^{(1)}$ (LO) and $\Gamma_{15^-}^{(2)}$ (LO)] can be observed at low temperature due to the stronger Fröhlich mechanism to Raman scattering.[21,32] The Raman experiments for the films at low temperatures (77–300 K) have been analyzed in detail.[21]

### B. Annealing effects on photoluminescence emissions

From Figures 3(a) and 3(b), the intensity of the PL signal for the $Cu_2O$ films increases with the annealing temperature under both the excitation wavelengths of 488 and 325 nm. The dramatic improvement in intensity is may be due to the defect during annealing conditions. There are some peaks located at about 1.52, 1.61, 1.94, 2, 2.28, 2.86, and 3.02 eV, which are labeled from $P_0$ to $P_6$ in order with increasing photon energy. It was reported that two main groups of PL signals have been identified: the free excitons and bound excitonic region extend from 450 to 650 nm (2.76–1.91 eV); the region of relaxed excitons at oxygen and copper vacancies extend from 630 to 1200 nm (1.97–1.03 eV).[34] Correspondingly, the peak at 1.72 eV can be assigned to the recombination of excitons bound to double charged oxygen vacancies ($V_o^{2+}$), and the band at 1.53 eV is produced by the recombination of bound excitons at single charged oxygen vacancy ($V_o^{+}$).[18,26] In order to determine the accurate peak positions under the 488 nm excitation, a curve fitting of the PL spectra for the $Cu_2O$ films in the photon energy range of 1.28–2.37 eV was carried out [Figure 3(c)]. The Gaussian multipeak fitting, including three separate bands [about 1.58–1.62 ($P_1$), 1.94–1.96 ($P_2$), and 2–2.07 ($P_3$) eV], is required to describe the profile satisfactorily. As seen in Figures 3(d) and 3(e), the three peak energies obviously shift to a high energy side with the annealing temperature and have maximal FWHM from the film at the highest annealing temperature. Note that the relative vacancy concentration is responsible for the adjustment of the 1.72 eV peak (mainly dominated by $V_o^{2+}$) and the one at 1.53 eV (mainly dominated by $V_o^{+}$). Furthermore, the peak intensities depend also on the corresponding radiative recombination efficiency.[26] It clearly shows the correlation between the PL bands and the relative concentration of the oxygen vacancies in the synthesized material. Therefore, the blueshift and broadening trend with the annealing temperature for peak $P_1$ indicate the decreasing in amount of $V_o^{+}$ and increasing in $V_o^{2+}$ correspondingly. In addition, the small emission shoulder at about 1.52 eV derived from $V_o^{+}$ appears in 325 nm excitation for the film annealed at 900 °C. It further suggests that the film annealed at 900 °C possess more oxygen vacancies, and the emission peak signal related to oxygen vacancy (such as $P_0$ and $P_1$) correspondingly increases.

Compared to the application of 488 nm, a similar emission at about 2 eV and the broadening variation with the annealing temperature can be observed for the excitation source using 325 nm. The 1.94–2.1 eV visible light is attributed to the direct recombination of the phonon-assisted excitons.[35,36] The broadening band at about 2.28 eV ($P_4$) might originate from to green emission[18] and the 2.86 eV ($P_5$) peak is due to the excitonic transitions from the different sub levels of the conduction band (CB) to the Cu *d*-shells of the valence band (VB).[37] The observed high-energy PL peak at 3.02 eV ($P_6$) should be associated with interband transitions

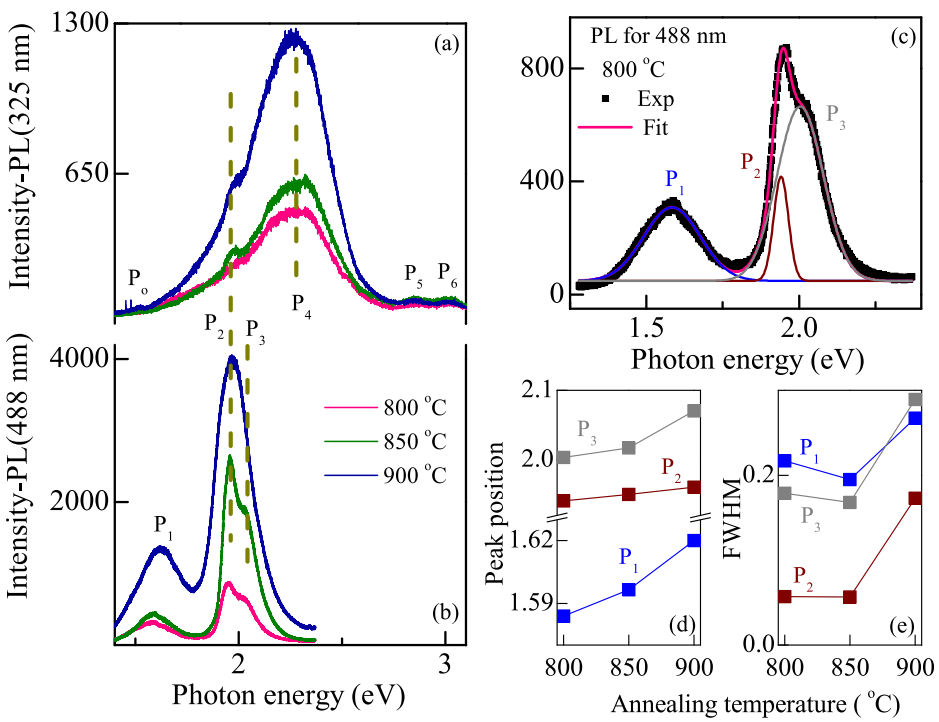


FIG. 3. (a) and (b) A comparison of photoluminescence spectra with 325 and 488 nm laser excitations at room temperature. The dashed lines indicate energy positions of the luminescence peaks. (c) For the excitation source using 488 nm, the positions of three emission peaks are obtained from the Gaussian fitting. The variations in the peak positions (d) and the full width at half-maximum (e) of $P_1$-$P_3$ for the $Cu_2O$ films with the annealing temperature at the application of 488 nm.

rather than the intra-atomic properties of impurities or defects.[18] It was reported that the peak at 3.03 eV revealed a red shift with increasing temperature from 22 to 300 K because the lattice parameter increased with increasing temperature.[18] The VB structure of $Cu_2O$ has Cu 3*d*, hybridized Cu 3*d*–4*s*, and O 2*p* character from angle resolved photoelectron spectroscopy.[38] The CB is derived from hybridized Cu 3*d*–4*s* and O 2*p* states. Transitions from the top of VB to the bottom of CB (3*d*–4*s*) are forbidden according to selection rules. Theoretically, it was predicted that transition from many bands below the top of VB to CB was negligible.[37] Thus, the relaxations of the electrons occur from the different subenergy levels of O 2*p* band to Cu 3*d* band, which give rise to the emissions at 2.86 and 3.02 eV. Moreover, Park *et al.* identified the peaks at 2.86 eV and 3.02 eV due to 4TO and 2TO phonon sidebands of 3.18 eV, which was attributed to quasi-direct transition caused by grain boundary-induced symmetry breaking.[18] This is because the TO and LO phonons with energies 75.5 and 78.7 meV (609 and 635 $cm^{-1}$) were reported from infrared absorption for $Cu_2O$, respectively.[11,39] Nevertheless, the values are much smaller than these derived by other literature using Raman scattering (e.g., TO, 78.5 meV; LO, 82.4 meV).[11,32,33] In the present work, the TO and LO components of the $\Gamma_{15^-}^{(2)}$ are difficult to be distinguished from Raman scatting at RT. However, the extracted energy (78.4 meV, 632 $cm^{-1}$, TO; 81.2 meV, 655 $cm^{-1}$, LO) for $\Gamma_{15^-}^{(2)}$ at 77 K can be obtained in our previous Raman experiments at low temperature.[21]

### C. Theoretical consideration and transmittance properties of the $Cu_2O$ films

Figure 4(a) shows the transmittance spectra of $Cu_2O$ films deposited under different annealing temperatures. It is pointed out that the spectral transmittance is larger than 25% in photon energy region of 2.5–6.5 eV due to the strong absorption for the $Cu_2O$ materials. Compared to other samples, the smaller transmittance at photon energy higher than 3 eV and the larger band gap near 2.2 eV can be observed for the $Cu_2O$ film annealed at 800 °C. There are two prominent dips in the range of 2–3 eV, which result from transitions to excitonic levels. Note that the average deviation of the two dip can be estimated to about 104 meV and the film grown under 800 °C has the largest variation for the above values, as seen in Figure 4(b). It can be believed that the spectral discrepancy is mainly ascribed to the different crystalline qualities and surface morphologies with annealing effect. In view of these results, the film annealed at 800 °C was chosen for temperature dependence studies due to the most remarkable excitonic features and stronger absorption at high energy, which are strongly related to the electronic band structure of the $Cu_2O$ crystal. As an example, the experimental transmittance spectra of the film recorded at 8 and 300 K are displayed in Figure 4(c), respectively. The intensities for all the dips reduce as the temperature increases, showing a remarkable response to the temperature. The narrow widths of the dips in the range of 2–3 eV at low temperature indicate the semiconductor nature of the direct-allowed exciton transitions.[40]

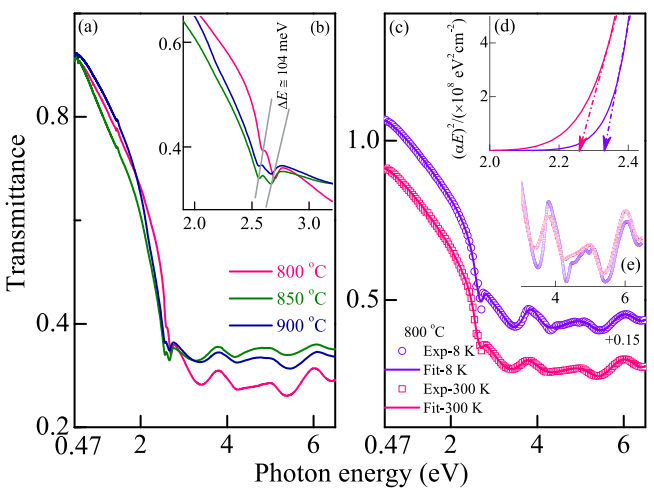


FIG. 4. (a) Experimental transmittance spectra of the $Cu_2O$ films at different annealing temperatures in the photon energy range of 0.47–6.5 eV. (b) The enlarged photon energy region for the excitonic transitions. (c) Experimental (dotted lines) and best fit (solid lines) transmittance spectra of the $Cu_2O$ film under 800 °C at temperatures of 8 and 300 K, respectively. Note that the transmittance spectra at 8 K are vertically shifted by adding 0.15 for clarification. (d) The band gap of the film from Tauc plots applied by the arrows. (e) The enlarged photon energy region from the transmittance spectra in order to observe some additional bands clearly.

Generally, the reliability of the fitting method mainly depends on the validity of the dielectric function model. The Tauc-Lorentz (TL) model is an available approach to describe the dielectric response of wide band gap materials in ultraviolet to near-infrared range, including the exciton effects. Moreover, the positions of electronic transitions can be accurately determined by the TL model, which are helpful to understand the absorption processes. The complex dielectric functions ($\varepsilon = \varepsilon_r + i\varepsilon_i$) of the $Cu_2O$ films can be expressed using the TL oscillator model[41,42]

$$\varepsilon_r(E) = \varepsilon_\infty + \frac{2}{\pi} P \int_0^\infty \frac{\xi \varepsilon_i(E)}{\xi^2 - E^2} d\xi, \tag{1}$$

$$\varepsilon_i(E) = \sum_{m=1}^{6} \frac{A_m E_{om} \Gamma_m (E - E_{tm})^2}{\left(E^2 - E_{om}^2\right)^2 + \Gamma_m^2 E^2} \frac{1}{E}, \tag{2}$$

where $\varepsilon_\infty$ is the high frequency dielectric constant, $P$ is the Cauchy principal part of the integral, $E$ is the incident photon energy, $A_m$, $E_{om}$, $\Gamma_m$, and $E_{tm}$ are the amplitude, peak position energy, broadening term, and Tauc gap energy of the $m$th oscillator, respectively. Based on the simulation of TL dielectric function to the experimental transmittance, the fitted parameter values at 8 and 300 K are summarized in Table I and the reproduced transmittance are also plotted in Figure 4(c) by the solid lines.

The dielectric functions of the $Cu_2O$ film can be uniquely determined by fitting the model function to the experimental data. The absorption coefficient can be calculated with $\alpha = 4\pi\kappa/\lambda$ and the order of magnitude is evaluated to be about $10^5$ $cm^{-1}$ at photon energy higher than 2 eV. The large value of absorption coefficient is an advantage for the band-edge absorption efficiency in $Cu_2O$ based solar cell. In addition, the power law behavior of Tauc is plotting of $(\alpha E)^2$ as a function of photon energy for the $Cu_2O$ films with direct

TABLE I. The Tauc-Lorentz's parameter values for the $Cu_2O$ films are determined from the simulation to ultraviolet-near-infrared transmittance spectra in Figure 4. Note that the $\varepsilon_\infty$ are estimated to 3.66 and 3.64 taken from the fitting results at 8 and 300 K, respectively.

| | 8 K | | | | 300 K | | | |
|---|---|---|---|---|---|---|---|---|
| Oscillator ($TL_m$) | $A_m$ | $E_{om}$ | $\Gamma_m$ | $E_{tm}$ | $A_m$ | $E_{om}$ | $\Gamma_m$ | $E_{tm}$ |
| $m=1$ | 7.62 | 2.676 | 0.24 | 1.95 | 32.96 | 2.638 | 0.29 | 2.34 |
| $m=2$ | 94.36 | 2.796 | 0.57 | 2.62 | 67.96 | 2.746 | 0.23 | 2.78 |
| $m=3$ | 8.82 | 3.428 | 0.79 | 2.09 | 19.04 | 3.247 | 1.37 | 1.91 |
| $m=4$ | 98.28 | 3.941 | 0.86 | 3.68 | 88.22 | 3.829 | 1.02 | 3.65 |
| $m=5$ | 1.74 | 5.458 | 0.88 | 2.38 | 2.01 | 5.404 | 0.90 | 2.74 |
| $m=6$ | 9.58 | 6.344 | 0.90 | 5.05 | 8.20 | 6.357 | 0.85 | 5.03 |

transition. The OBG is determined from the intercept of the straight-line portion of the Tauc's plots at $\alpha=0$, as shown in Figure 4(d). It can be found that the OBG value decreases from 2.33 to 2.26 eV with increasing the temperature from 8 to 300 K, which indicates that the OBG has a negative temperature coefficient. The values are slightly smaller than that (2.39 eV) of $Cu_2O$ films by reactive magnetron sputtering,[43] but higher than the conventional one of 2.1 for $Cu_2O$.[44]

Moreover, the line shape of refraction index ($n$) is similar to that in $Cu_2O$ single crystal determined by spectroscopic ellipsometry.[19] The $n$ increases with the photon energy and approaches the maximum at 2.6 eV, then decreases and displays some peaks with further increasing photon energy. At the limited energy of 0.47 eV, the evaluated $n$ is around 2.33 and 2.32 at 8 and 300 K, respectively, which are slightly smaller than reported value (2.58 at 0.5 eV).[44] The $n$ values are significantly affected by the temperature and show a decreasing trend with increasing temperature in the photon energy range of 0.47–6.5 eV. This is because the OBG for the film has a negative temperature coefficient and becomes narrower with increasing temperature. Therefore, the incident photons will likely excite electrons from the VB to the CB and result in the strong absorption at the photon energies above the band gap, which can induce a lower dielectric function with the temperature. Figure 6(a) shows the $n$ with the temperature at the photon energy of 0.47, 3, and 5 eV, respectively. From the variations of the three parameters, with increasing the temperature, all values have a remarkable reduction at the low temperature and almost kept as a constant at the temperature higher than 100 K. While the high frequency dielectric constant abruptly decreases until the temperature rises up to 100 K. It indicates the change in the crystalline and electronic band structure occurs as the temperature near 100 K for the film. The anomalies have been recorded from the temperature dependence of lattice constant for $Cu_2O$ material during both cooling and heating processes. The temperature close to 80 K associated with a small contraction/expansion of the cubic lattice.[11] In addition, extended x-ray absorption fine structure (EXAFS) data on intranetwork and internetwork Cu-Cu distances also suggest different thermal expansions of these bonds above 100 K.[12,45]

### D. Electronic band structures and transitions at low temperature

Interestingly, the behavior for the absorption coefficient of the $Cu_2O$ is rather spectacular, especially for the contribution of exciton series and high energy transitions. Base on the fitting results, six transitions at the photon energy from ultraviolet to near-infrared can be clearly identified from the absorption coefficient spectra and labeled as $E_{o1}$–$E_{o6}$ in order (Figure 5). In the $Cu_2O$ material, both the extreme of the lowest CB and that of the highest VB are located at the $\Gamma$ point in the Brillouin zone, forming a direct energy gap. The highest VB dominated by the Cu 3 d states splits into an upper $\Gamma_7^+$ band and a lower $\Gamma_8^+$ band due to the spin-orbit interaction ($\Delta_{SO}=124$ meV).[18,40] Since the lowest CB $\Gamma_6^+$ and the split VBs ($\Gamma_7^+$ and $\Gamma_8^+$) mainly have Cu 3 s and Cu 3 d characters, respectively, the transitions between them ($\Gamma_6^+$–$\Gamma_7^+$, $\Gamma_6^+$–$\Gamma_8^+$ so-called yellow and green transitions) are all parity forbidden.[40] Note that no peaks around 2.15 and 2.25 eV, from the exciton series of the yellow and green transitions, are clearly observed in temperature-dependent transmittance for the $Cu_2O$ crystals. This is because of the small oscillator strengths for the forbidden transitions of the yellow and green transitions.[40] However, the absorption above 2.0 eV gradually increases with the photon energy (seen Figure 5), which indicates that the lowest excitonic transition in the range of 2.0–2.3 eV is weakly allowed via phonon-assisted processes that relax the selection rules. Moreover, the second-lowest CB having the allowed parity $\Gamma_8^-$ is located very close to the lowest CB, i.e., only 0.558 eV higher. The transitions between the second-lowest CB and the split VBs ($\Gamma_7^+$–$\Gamma_8^-$, $\Gamma_8^+$–$\Gamma_8^-$ so-called blue and indigo transitions) are direct and allowed.[20,40] Hence, $Cu_2O$ reveals strong exciton absorption peaks around 2.6 eV. In the present case, two prominent shoulders appear at near 2.6 and 2.7 eV, even remain at RT, which result from transitions to excitonic levels. The former features between the peculiar second-lowest CB $\Gamma_8^-$ and the split VBs (an upper $\Gamma_7^+$ band and a lower $\Gamma_8^+$ band) can be regarded as blue ($\Gamma_7^+ \rightarrow \Gamma_8^-$) and indigo ($\Gamma_8^+ \rightarrow \Gamma_8^-$) exciton

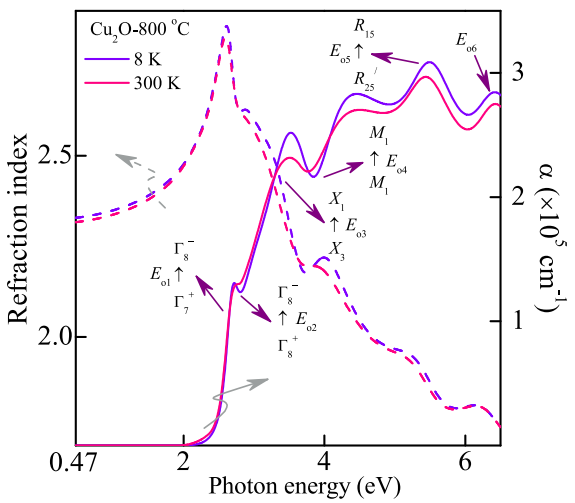


FIG. 5. The refraction index (dotted curves) and absorption coefficient (solid curves) at 8 and 300 K for the $Cu_2O$ film with anneal temperature of 800 °C, respectively. The arrows indicate the physical origin and energy positions of the electronic transitions.

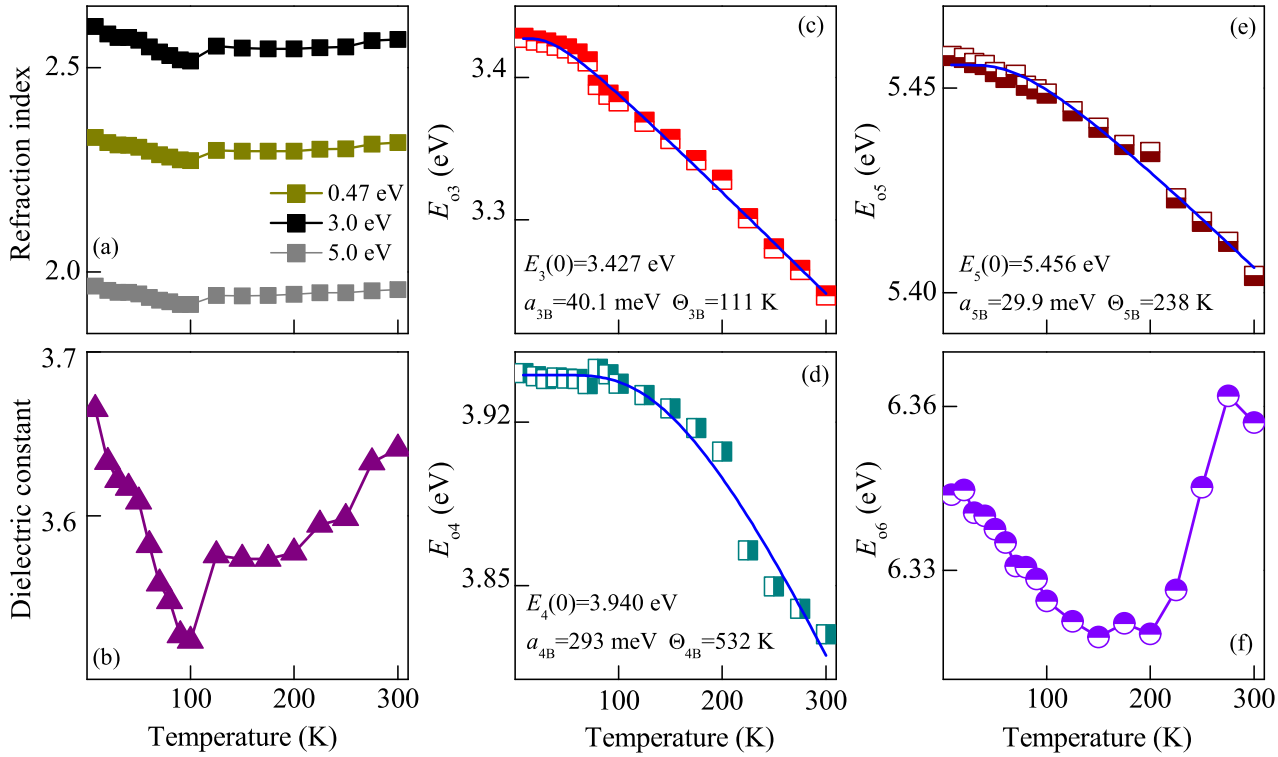


FIG. 6. The temperature dependence of (a) refractive index at photon energies of 0.45, 3, and 5 eV, (b) high frequency dielectric constant, (c) electronic transition energies of $E_{03}$, (d) $E_{04}$, (e) $E_{05}$, and (f) $E_{06}$ for the $Cu_2O$ film grown under 800 °C, respectively. The solid curves are the fitting results with the Bose-Einstein model.

states, respectively. The difference between them is estimated to be about 120 meV and 108 meV at 8 and 300 K, respectively, which are slightly smaller than the split value ($\Delta_{SO} = 124$ meV) due to the spin-orbit interaction.[40]

The major structures in higher energy labeled as $E_{o3}$, $E_{o4}$, and $E_{o5}$ can be accounted for specific band-to-band transitions. The broadening bands in order are ascribed to $X_3 \rightarrow X_1$, $M_1 \rightarrow M_1$, and $R'_{25} \rightarrow R_{15}$ transitions for the $Cu_2O$ sample, respectively.[40,46] From spectral transmittance experiments [seen Figure 4(e)], some additional bands between 4.27 and 5.41 eV could be observed due to a complex electronic structure of the $Cu_2O$ film. These bands become much stronger and more distinct at the lowest temperature. It is found that these ultraviolet bands may be assigned to the transitions from the copper *d*-shells to the higher sublevels of CB.[47] Absorption in the 215–250 nm (5.76–4.96 eV) range has been characterized by the 3 *d*–4 *s* transition of isolated $Cu^+$ ions.[48]

Figures 6(c)–6(f) show the temperature evolutions of the $E_{o3}$–$E_{o6}$ electronic transitions. With increasing the temperature, the red shift trend of $E_{o3}$–$E_{o5}$ transition energy can be found and the total deviation of transition energy is 181, 112, and 54 meV, respectively, with the order of electronic transitions. It indicates that the electronic band structure is generally modified corresponding to the temperature, which has a greater effect on the $E_{o3}$ transition. Note that the variation tendency in $E_{o3}$, $E_{o4}$, and $E_{o5}$ with the temperature can be expressed by the Bose-Einstein model: $E(T) = E(0) - 2a_B/[\exp(\Theta_B/T) - 1]$, where $E(0)$ is the energy at 0 K, $a_B$ is the strength of the coupling interaction, $\Theta_B \equiv \hbar\nu/k_B$ is the characteristic temperature representing the effective phonon energy on the temperature scale, and $T$ is the experimental temperature. The obtained results display that the strengths of $a_B$ and $\Theta$ in the $E_{o4}$ transition ($a_B = 293$ meV, $\Theta = 532$ K) are stronger than those in the $E_{o3}$ ($a_B = 40.1$ meV, $\Theta = 111$ K) and $E_{o5}$ ($a_B = 29.9$ meV, $\Theta = 238$ K) transitions. It indicates that the temperature influences on the strength of different optical transitions are disparate. Furthermore, the parameters of $a_B$ and $\Theta$ in the $E_{o3}$ and $E_{o5}$ transitions are smaller than those from the OBG energy for the $CuGaO_2$ semiconductor film ($a_B = 68.9$ meV and $\Theta = 296.2$ K).[23]

However, the highest order transition $E_{o6}$ does not follow the Bose-Einstein relationship, which can be described by an interband transition from the occupied Cu 3 *d* state to the unoccupied states with mixed Cu 3 *d*, 4 *s*, and O 2 *p* character.[49] The obtained value of the $E_{o6}$ transition is very close to that (6.33 eV) in an extended spectral range up to 10 eV reported by spectroscopic ellipsometry measurements.[19] Moreover, the $E_{o6}$ transition energy decreases from 6.344 to 6.318 eV, corresponding to increasing the temperature from 8 to 200 K, which indicates that the total redshift value of the $E_{o6}$ is about 26 meV. Based on the abrupt variations with the further increase in temperature, it can be easily recognized that the anomalous behavior from the $E_{o6}$ transition takes place at about 200 K for the $Cu_2O$ film. The finding is similar to the anomalous temperature from Raman scattering in $Cu_2O$, which may be related to structural or electronic changes and further influence the thermal expansion behavior above 190 K.[11] It is also reported that the cell parameter *a* of $Cu_2O$ decreases when the temperature is varied from

liquid helium temperature to 200 K and remains virtually constant from 200 to 300 K.[50] Therefore, one can conclude that the electronic orbital hybridization and band splitting can be strongly affected by the temperature, which result in the modification of electronic band structures for the $Cu_2O$ film.

## IV. SUMMARY

To summarize, the evolution of the microstructure, electronic band, and electrical transition properties have been investigated by XRD, Raman scattering, PL, and temperature dependent transmittance measurement for the $Cu_2O$ films prepared under various annealing temperatures. The peak positions of Raman phonon modes agree well with those of the typical phonon vibrations for $Cu_2O$ crystal. The most intense Raman signal for all $Cu_2O$ films at RT is the second-order overtone $2\Gamma_{12^-}$, indicating the existence of strong electron-phonon coupling mediated by Fröhlich interaction. Note that the LO-TO splitting of the $\Gamma_{15^-}^{(2)}$ could be distinguished in the Raman scattering at RT. From direct comparison of PL spectra with 488 and 325 nm laser excitations, the electronic transition energies and intensities are shown to present the annealing-temperature dependent behavior. There are minimum values at near 100 K for both the refraction index and high frequency dielectric constant. Six transitions can be clearly identified and $E_{o3}$–$E_{o5}$ transition energies decrease with increasing the temperature. Moreover, it can be found that the anomalous behavior takes place at about 200 K from the $E_{o6}$ transition for the $Cu_2O$ sample. It can conclude that the temperature contributions are responsible for the adjustment of electronic band structures and result in different optical response behaviors for the $Cu_2O$ films. The present results indicate that the $Cu_2O$-based materials can be suitable for some optoelectronic applications.

## ACKNOWLEDGMENTS

This work was financially supported by Major State Basic Research Development Program of China (Grant Nos. 2011CB922200 and 2013CB922300), Natural Science Foundation of China (Grant Nos. 11374097, and 61376129), Projects of Science and Technology Commission of Shanghai Municipality (Grant Nos. 14XD1401500, 13JC1402100, and 13JC1404200), and the Program for Professor of Special Appointment (Eastern Scholar) at Shanghai Institutions of Higher Learning. One of the authors (Wen Lei Yu) thanks the support from Project of Wenzhou Medical University (Grant No. QTJ14012).

[1]L. Hu, Y. M. Huang, F. P. Zhang, and Q. W. Chen, Nanoscale **5**, 4186 (2013).
[2]Q. Li, P. Xu, B. Zhang, H. Tsai, S. J. Zheng, G. Wu, and H. L. Wang, J. Phys. Chem. C **117**, 13872 (2013).
[3]C.-H. Kuo and M. H. Huang, Nano Today **5**, 106 (2010).
[4]C. M. McShane and K.-S. Choi, Phys. Chem. Chem. Phys. **14**, 6112 (2012).
[5]Y. L. Liu, G. J. Yang, H. Zhang, Y. Q. Cheng, K. Q. Chen, Z. Y. Peng, and W. Chen, RSC Adv. **4**, 24363 (2014).
[6]K. Han and M. Tao, Sol. Energy Mater. Sol. Cells **93**, 153 (2009).
[7]A. Mittiga, E. Salza, F. Sarto, M. Tucci, and R. Vasanthi, Appl. Phys. Lett. **88**, 163502 (2006).
[8]L. M. Wong, S. Y. Chiam, J. Q. Huang, S. J. Wang, J. S. Pan, and W. K. Chim, J. Appl. Phys. **108**, 033702 (2010).
[9]S. W. Lee, Y. S. Lee, J. Heo, S. C. Siah, D. Chua, R. E. Brandt, S. B. Kim, J. P. Mailoa, T. Buonassisi, and R. G. Gordon, Adv. Energy Mater. **4**, 1301916 (2014).
[10]X. D. Xiao, L. Miao, G. Xu, L. M. Lu, Z. M. Su, N. Wang, and S. Tanemura, Appl. Surf. Sci. **257**, 10729 (2011).
[11]M. Ivanda, D. Waasmaier, A. Endriss, J. Inhringer, A. Kirfel, and W. Kiefer, J. Raman Spectrosc. **28**, 487 (1997).
[12]R. Mittal, S. L. Chaplot, S. K. Mishra, and P. P. Bose, Phys. Rev. B **75**, 174303 (2007).
[13]Y. S. Lee, M. T. Winkler, S. C. Siah, R. Brandt, and T. Buonassisi, Appl. Phys. Lett. **98**, 192115 (2011).
[14]H. Z. Bao, Z. H. Zhang, Q. Hua, and W. X. Huang, Langmuir **30**, 6427 (2014).
[15]Y. X. Zhao, W. T. Wang, Y. P. Li, Y. Zhang, Z. F. Yan, and Z. Y. Huo, Nanoscale **6**, 195 (2014).
[16]B. Sinha, T. Goswami, S. Paul, and A. Misra, RSC Adv. **4**, 5092 (2014).
[17]J. H. Jung, T. W. Kim, M. S. Song, Y.-H. Kim, and K. H. Yoo, J. Appl. Phys. **101**, 093708 (2007).
[18]J. W. Park, H. Jang, S. Kim, S. H. Choi, H. Lee, J. Kang, and S. H. Wei, J. Appl. Phys. **110**, 103503 (2011).
[19]F. Haidu, M. Fronk, O. D. Gordan, C. Scarlat, G. Salvan, and D. R. T. Zahn, Phys. Rev. B **84**, 195203 (2011).
[20]W. Y. Ching, Y.-N. Xu, and K. W. Wong, Phys. Rev. B **40**, 7684 (1989).
[21]W. L. Yu, M. J. Han, K. Jiang, Z. H. Duan, Y. W. Li, Z. G. Hu, and J. H. Chu, J. Raman Spectrosc. **44**, 142 (2013).
[22]L. Armelao, D. Barreca, M. Bertapelle, G. Bottaro, C. Sada, and E. Tondello, Thin Solid Films **442**, 48 (2003).
[23]M. J. Han, K. Jiang, J. Z. Zhang, Y. W. Li, Z. G. Hu, and J. H. Chu, Appl. Phys. Lett. **99**, 131104 (2011).
[24]K.-P. Bohnen, R. Heid, L. Pintschovius, A. Soon, and C. Stampfl, Phys. Rev. B **80**, 134304 (2009).
[25]M. Tiano, M. Dapiaggi, and G. Artioli, J. Appl. Crystallogr. **36**, 1461 (2003).
[26]H. Solache-Carranco, G. Juárez-Díaz, A. Esparza-García, M. Briseño-García, M. Galván-Arellano, J. Martínez-Juárez, G. Romero-Paredes, and R. Peña-Sierra, J. Lumin. **129**, 1483 (2009).
[27]D. Powell, A. Compaan, J. R. Macdonald, and R. A. Forman, Phys. Rev. B **12**, 20 (1975).
[28]F. M. Li, R. Waddingham, W. I. Milne, A. J. Flewitt, S. Speakman, J. Dutson, S. Wakeham, and M. Thwaites, Thin Solid Films **520**, 1278 (2011).
[29]Y. Petroff, P. Y. Yu, and Y. R. Shen, Phys. Rev. B **12**, 2488 (1975).
[30]N. A. Mohemmed Shanid, M. Abdul Khadar, and V. G. Sathe, J. Raman Spectrosc. **42**, 1769 (2011).
[31]A. Sanson, Solid State Commun. **151**, 1452 (2011).
[32]A. Z. Genack, H. Z. Cummins, M. A. Washington, and A. Compaan, Phys. Rev. B **12**, 2478 (1975).
[33]M. Jörger, T. Fleck, C. Klingshirn, and R. V. Baltz, Phys. Rev. B **71**, 235210 (2005).
[34]T. Ito and T. Masumi, J. Phys. Soc. Jpn. **66**, 2185 (1997).
[35]M. Izaki, S. Sasaki, F. B. Mohamad, T. Shinagawa, T. Shinagawa, T. Ohta, S. Watase, and J. Sasano, Thin Solid Films **520**, 1779 (2012).
[36]Y. L. Liu, Y. C. Liu, R. Mu, H. Yang, C. L. Shao, J. Y. Zhang, Y. M. Lu, D. Z. Shen, and X. W. Fan, Semicond. Sci. Technol. **20**, 44 (2005).
[37]K. Das, S. N. Sharma, M. Kumar, and S. K. De, J. Appl. Phys. **107**, 024316 (2010).
[38]A. Önsten, M. Månsson, T. Claesson, T. Muro, T. Matsushita, T. Nakamura, T. Kinoshita, U. O. Karlsson, and O. Tjernberg, Phys. Rev. B **76**, 115127 (2007).
[39]P. Dawson, M. M. Hargreave, and G. R. Wilkinson, J. Phys. Chem. Solids **34**, 2201 (1973).
[40]H. Amekura, N. Umeda, Y. Takeda, and N. Kishimoto, Appl. Phys. Lett. **89**, 223120 (2006).
[41]G. E. Jellison, Jr. and F. A. Modine, Appl. Phys. Lett. **69**, 371 (1996).
[42]W. L. Yu, W. W. Li, J. D. Wu, J. Sun, Z. G. Hu, and J. H. Chu, J. Appl. Phys. **110**, 123502 (2011).
[43]E. Fortunato, V. Figureueiredo, P. Barquinha, E. Elamurugu, R. Barros, G. Goncalves, S.-H. K. Park, C.-S. Hwang, and R. Martins, Appl. Phys. Lett. **96**, 192102 (2010).

[44]C. Malerba, F. Biccari, C. L. A. Ricardo, M. D'Incau, P. Scardi, and A. Mittiga, Sol. Energy Mater. Sol. Cells **95**, 2848 (2011).
[45]A. Sanson, F. Rocca, G. Dalba, P. Fornasini, R. Grisenti, M. Dapiaggi, and G. Artioli, Phys. Rev. B **73**, 214305 (2006).
[46]A. Nath and A. Khare, J. Appl. Phys. **110**, 043111 (2011).
[47]S. Jana and P. K. Biswas, Mater. Lett. **32**, 263 (1997).
[48]A. Oliver, J. C. Cheang-Wong, J. Roiz, J. M. Hernández, L. Rodríguez-Fernández, and A. Crespos, Nucl. Instrum. Methods Phys. Res. B **175–177**, 495 (2001).
[49]Y.-J. Kim, J. P. Hill, H. Yamaguchi, T. Gog, and D. Casa, Phys. Rev. B **81**, 195202 (2010).
[50]M. Dapiaggi, W. Tiano, G. Artioli, A. Sanson, and P. Fornasini, Nucl. Instrum. Methods Phys. Res. B **200**, 231 (2003).